A lubrication analysis of pharyngeal peristalsis: Application to flavour release

Clément de Loubens, Albert Magnin, Eric Verin, Marion Doyennette, Ioan Cristian Tréléa, Isabelle Souchon

www.elsevier.com/locate/yjtbi

A lubrication analysis of pharyngeal peristalsis: Application to flavour release

Clément de Loubens, Albert Magnin, Eric Verin, Marion Doyennette, Ioan Cristian Tréléa, Isabelle Souchon

PII: S0022-5193(10)00469-8
DOI: doi:10.1016/j.jtbi.2010.09.003
Reference: YJTBI6143

To appear in: *Journal of Theoretical Biology*

Received date: 19 May 2010
Revised date: 1 September 2010
Accepted date: 1 September 2010

Cite this article as: Clément de Loubens, Albert Magnin, Eric Verin, Marion Doyennette, Ioan Cristian Tréléa and Isabelle Souchon, A lubrication analysis of pharyngeal peristalsis: Application to flavour release, *Journal of Theoretical Biology*, doi:10.1016/j.jtbi.2010.09.003

A lubrication analysis of pharyngeal peristalsis: application to flavour release

Clément de Loubens[a,b,*], Albert Magnin[c], Eric Verin[d], Marion Doyennette[a,b], Ioan Cristian Tréléa[b,a], Isabelle Souchon[a,b]

[a] *INRA, UMR 782 Génie et Microbiologie des Procédés Alimentaires, CBAI 78850 Thiverval Grignon, France*
[b] *AgroParisTech, UMR 782 Génie et Microbiologie des Procédés Alimentaires, CBAI 78850 Thiverval Grignon, France*
[c] *Laboratoire de Rhéologie, Université Joseph Fourier-Grenoble I, Grenoble INP, CNRS (UMR 5520), BP 53, Domaine Universitaire, 38041 GRENOBLE cedex 9, France*
[d] *Department of Physiology, Rouen University Hospital, 1 rue de Germont, 76031 Rouen Cedex, France*

Abstract

After eating a liquid or a semi-liquid food product, a thin film responsible for the dynamic profile of aroma release coats the pharyngeal mucosa. The aim of this article was to analyze the fluid mechanics of pharyngeal peristalsis and to develop a simple biomechanical model in order to understand the role of saliva and food bolus viscosity on the coating of pharyngeal mucosa. We began by analysing the physiology and the biomechanics of swallowing in order to determine relevant model assumptions. This analysis of the literature clarified the types of mechanical solicitations applied on the food bolus. Moreover, we showed that the pharyngeal peristalsis in the most occluded region is equivalent to a forward roll coating process, the originality of which is lubrication by a film of saliva. A model based on the lubrication theory for Newtonian liquids was developed in dimensionless form. The parametric study showed the strong influence of relative saliva thickness on the food bolus coating. A specific experimental device was designed that confirms the model predictions. Two sets of conditions that depend on the relative thickness of saliva were distinguished. The first is characterised by a relatively thin film of saliva: food bolus viscosity has a strong impact on mucosa coating. These phenomena are well represented by the model developed here. The second is obtained when the saliva film is relatively thick: hydrodynamic mixing with saliva, interdiffusion or instabilities may govern mucosa coating. Finally, these results were extrapolated to determine the

*Corresponding author
Email addresses: cdeloubens@grignon.inra.fr (Clément de Loubens), magnin@ujf-grenoble.fr (Albert Magnin), Eric.Verin@chu-rouen.fr (Eric Verin), souchon@grignon.inra.fr (Isabelle Souchon)

influence of food bolus viscosity on the dynamic profile of flavour release according to physiological parameters.

Keywords: biomechanics, swallowing, aroma, viscosity, pharynx, saliva, food bolus

1. Introduction

Increasing attention has been given to the analysis and modelling of biomechanical phenomena related to oral food processing over the last five years. More and more studies have been dedicated to integrating physiological and biomechanical constraints into the formulation of food to improve care for dysphagia patients [1–3] as well as into the formulation of health food with control of flavour and texture perception [4–10]. Improving the nutritional quality of foods without modifying their organoleptic properties is a real challenge that requires more knowledge about the mechanisms involved in sensorial stimulus release in terms of both products and consumers.

After eating a liquid or a semi-liquid food product, a thin film responsible for the dynamic profile of aroma release coats the pharyngeal mucosa [11, 12]. The phenomena governing pharyngeal mucosa coating are insufficiently understood. Many studies hypothesize that the rheological properties of the food bolus modify the coating and, subsequently, the dynamic profile of flavour release [13–16]. However, there is no consensus on the role played by physical effects such as pharyngeal mucosa coating and that of sensory interactions between texture and aroma. For example, the complex viscosity of flavoured yogurts has a direct influence on both the perception and dynamic profile of flavour release [16], while the viscosity of flavoured hydrocolloid solutions influences perception but not the dynamic profile of flavour release [13, 17]. Moreover, investigations of the influence of viscosity on postdeglutitive pharyngeal residue are not in agreement [18–20]. The relationship between viscosity and post-deglutitive pharyngeal residue is not clear. Residue was evaluated by different techniques such as scintigraphy or fibreoptic endoscopic evaluation. The retention of products on mucosa can be analysed by fluorescence as well [21]. Results seem to be dependent on the method chosen and probably on the individual. We therefore need to develop other approaches to analyse and understand the phenomena governing pharyngeal mucosa coating.

For this purpose, Weel et al. [15] developed an "artificial throat" in which liquids were poured down a tube and a thin film coated the tube wall. Their results confirmed the importance of coating for aroma release, but the flow was governed by gravity, whereas *in vivo*, the liquid is forced by pharyngeal peristalsis.

The aim of this study was to develop a simple biomechanical model of pharyngeal peristalsis that focuses on the food bolus coating of the mucosa. We first analysed the physiology and the biomechanics of swallowing in order to determine relevant model assumptions. On the basis of this analysis, we considered that the physiological process is equivalent to a forward roll coating process, the originality of which is lubrication by saliva. Second, a mathematical model based on a lubrication analysis for Newtonian liquids was developed. A specific experimental device was designed to confirm model predictions. The influence of food bolus viscosity and lubrication by saliva on mucosa coating and the forces generated was then shown. Finally, the results obtained were applied in order to assess the impact of food bolus viscosity on flavour release.

2. The physiology of swallowing and biomechanical analysis

2.1. Anatomy

The pharynx extends from the nasal cavity to the pharyngoesophageal segment [22]. It can be divided into three parts: the naso-, the oro- and the hypopharynx (Figure 1). The oropharynx, that extends from the palate to the tongue base at the level of the epiglottis and is at the croosroads where the residual product and the breath flow come in contact. It is therefore a key element in flavour release.

2.2. Swallowing sequences

After being chewed and mixed with saliva, the food bolus is propelled by the tongue into the oropharynx (Figure 2: phase 1). Several succesive phenomena are observed: i- the pharynx riszes, ii- the bolus tail enters the pharynx, iii- the upper oesophageal sphincter opens and the tongue base and the pharyngeal constrictors generate a peristaltic wave (Figure 2: phase 2). Bolus propulsion is due to the opposition of the tongue base with constrictors and the progressive forward movement of the posterior pharyngeal wall [23]. It is mediated by an involuntary reflex [24]. The wave velocity is between 0.1 and 0.5 m/s [1, 2, 24, 25]. During this phase, the highest frictional forces are generated in the most occluded region of the constriction [26]. Visualisation by X-rays attests to the existence of a thin film of product coating the oropharyngeal mucosa [11] that can be explained by a reflux of the food bolus in the opposite direction of the peristaltic wave (Figure 2).

2.3. Physical representation of the pharyngeal peristalsis

Many authors have studied peristaltic flows in the gastrointestinal tract. Gregersen [27] made a brief review of these studies. All of these studies focused on the global flow generated by peristaltic

waves but not in coating phenomena resulting from a single wave. Numerical models have already been proposed to simulate the swallowing of a liquid bolus [1, 2] and a gelled bolus [3] in order to calculate the evolution of pressure and flow rates. The length scale used is the oropharynx width (∼30 mm) that does not permit us to observe local phenomena such as coating (∼10 µm). In order to model this phenomenon, in the present study, we only considered the most occluded region of the wave. Firstly, this is the zone where there may be a reflux: a weak amount of food bolus flows in the opposite direction of the peristaltic wave that leads to coating of the mucosa. Secondly, as analysed by Pal et al. [26], the strongest frictional forces are generated in this zone. We considered a peristaltic wave (Figure 3) and its associated frame of reference. Within this framework and near the most occluded point, the two pharyngeal walls are in rotation, each one in relation to the other. Thus, two forward roll cylinders can simplify the peristaltic movement. The two rolling cylinders represent the contact between the tongue-base and the posterior pharyngeal wall in the oropharynx. This simplification is not a complete representation of the swallowing, but only a physiological realistic schematisation of the phenomena that permit to generate a thin film of product after swallowing. In the physiological case of swallowing, a thin saliva film lubricates the mucosa. From a tribological point of view, we made the hypothesis that we are always in a hydrodynamic regime, in other words, the film generated is thick enough to avoid contact between the two walls [28]. If this was not the case, it would lead to a boundary regime (walls in contact): friction would be great and the mucosa could be damaged. In order to model the fluid dynamics of such a problem, the main challenge is to determine the kind of mechanical solicitations applied by the pharyngeal constrictors and by the base of the tongue and to determine boundary conditions that are consistent with physiology.

2.4. Mechanical solicitations

Contraction of pharyngeal constrictors is due to the active shortening of the muscles fibres by the effects of nerves [27]. It results from this shortening a distribution of stress and strain in the muscles that is transmitted to the fluid through boundary conditions, but the fluid sets against this contraction by the generation of opposite forces. The type of solicitations imposed by the pharyngeal constrictors and by the base of the tongue remains an open question. The nerve simulation is like the same state of stress or strain is always imposed to the fluid? What governs the velocity of the wave? Are these solicitations stationary or are they dependent on the position?

In the contact created by the two cylinders, a hydrodynamic pressure profile is generated which that depends on the boundary pressure conditions [28]. The integration of its profile generates a normal force that separates the two cylinders, the lift (or load) L' (Figure 3). In order to determine the order of magnitude of this lift, intraluminal manometric data can be used. These measurements are often used during diagnosis and can help in understanding muscle activity, but interpretation remains difficult. Practitioners collect manometric data using a 4-mm-diameter catheter with ten recording points and measure space-time pressure structure during swallowing [29]. A relevant interpretation makes it possible to estimate the passive and active tension in the hollow organ walls [30]. Considering that the catheter does not influence pharyngeal constrictor response, the pressure profile integration makes it possible to determine the generated lift L' in the contact between the catheter and the mucosa. A possible way of determining the type of solicitation imposed by muscles is to change bolus consistency.

Few studies have recorded pressure during swallowing for different bolus consistencies. Some authors saw no significant effects of consistency on the maximal pressure measured in the oropharynx between water, pudding and potatoes [31] or between barium boluses with different viscosities [25, 32, 33] while others saw differences between water, pudding and buttered bread [34]. This maximal pressure depends on the position in the oropharynx [29, 34]. The values mentioned were between 20 and 30 kPa [25, 29, 33–35]. By integrating the obtained pressure profile measured by Williams et al. [29], we can estimate a load of about 10-60 N per unit of width.

The second question is to determine whether there is a mechanism that regulates wave velocity. Tail bolus velocity, which corresponds to the pharyngeal peristalsis wave, has also been compared with consistency, but the results between studies are not coherent. Dantas et al. [25] showed that the greater the consistency was, the shorter the wave duration was. Variations range from 0.35 to 0.45 s. Taniguchi et al. [36] noted that the wave is slower for syrups than for water or agar gels. However the same team [37] saw no effects of consistency with the same products. Ali et al. [32] showed that the oral and pharyngeal mucosal receptors regulate the duration of the midpharyngeal contraction, which is reduced by 29% by oral-pharyngeal anesthesia. From these observations, we can suppose that the wave velocity is regulated by the pharyngeal mechanoreceptors response. In the contact between the two walls, shear stress acts on the mucosa and hence on the mechanoreceptors. In a shear flow, the order of magnitude of this stress is about $\mu' U'/H'_0$, where μ' is the food bolus viscosity (Pa.s), U' the wave velocity (m/s) and H'_0 the gap between the mucosa (m).

We can thus hypothesize that the wave velocity is modulated in order to avoid mucosa damage caused by the action of shear stress on the wall mucosa referred to a drag D' (in N per unit of width, Figure 3).

Although all of the studies are not in agreement, we can reasonably assume that pharyngeal constrictors impose a constant load, and that the velocity is modulated in order not to exceed a constant drag. In this study, we numerically treated the first case at an imposed gap and velocity. From a modeling point of view, it is more convenient to set the gap and the velocity and to calculate the load and the drag. In order to carry out qualitative and quantitative applications, rearranging the results obtained allowed us to treat the second case at an imposed load and drag.

2.5. Boundary conditions

Boundary conditions consistent with physiology must be defined. The presence of a film-splitting region at the output contact was taken into account [38]. We considered that the contact is fully flooded by food bolus upstream and that the upper oesophageal sphincter is fully open and does not create an overpressure. Manometric recording validates this hypothesis for non-pathological cases [29]. No wall slip between pharyngeal mucosa and saliva was considered. In this study, we principally investigated the influence of the viscosity ratio α of the food bolus on saliva and of the initial thickness of saliva t_1' on flow rates and on the generated forces (L' and D'). Mucosa deformability is thus ignored in the initial approach. We will discuss of its importance later.

Table 1 summarises the values of the physiological parameters.

3. Lubrication model of pharyngeal peristalsis

3.1. Physical formulation

The thin film formation is dominated by the phenomena that act in the contact zone between the base of the tongue and the posterior pharyngeal wall. Thus, the characteristic length useful in our problem to define the Reynolds number Re is the minimum half gap between the walls H_0' ($\approx$10µm) and we have:

$$Re = \frac{\rho U' H_0'}{\mu'} \tag{1}$$

where ρ is the fluid density (10^3kg/m3),U' the wave velocity (0.2 m/s) and μ' the viscosity that ranges between 10^{-3}Pa.s (water) and the infinity. So, depending of the fluid viscosity, Re is

included between 0 and 2. The lubrication approximation is appropiate if the Reynolds number Re is very small compared to the ratio of the the characteristic length of the contact approximately $\sqrt{2R'H'_0}$ on the width of the contact H'_0 [28]:

$$Re << \frac{\sqrt{2R'H'_0}}{H'_0} \tag{2}$$

The value of the ratio $\sqrt{2R'H'_0}/H'_0$ is about 90 and the inertial terms can be neglected compared to the viscous term in the Navieer-Stokes equation.

The time scale of the flow is given by the ratio of the characteristic length of the contact approximately $\sqrt{2R'H'_0}$, -where R is the roll radius (0.04 m)- on the wave velocity U'(0.2m/s). Thus this time scale is about 4 ms and is very short compared to the time scale of the pharyngeal phase (typically 0.5 s) to neglect the non stationary term of the Navier-Stokes equations. Thus, we can use the lubrication approximation to model this flow [28]. Moreover, we suppose that the mechanical solicitations applied by the constrictors are stationary during the pharyngeal phase. This last assumption could be refined with more experimental data.

The general features of rigid roll coating operations have been described by Coyle et al. [38]. They gave analytical solutions for different boundary conditions in the monolayer case. Hannachi et Mitsoulis [39] studied the multilayer case applied to the calendering with boundary conditions specific to their problem. The present physical situation was modelled with the lubrication approximation for Newtonian liquids. In addition, the presence of a lubricating saliva film and of a film-splitting region at the output contact were taken into account.

The geometry is symmetric (Figure 4). Relative quantities associated with saliva and the food bolus are referred to as noted 1 and 2, respectively. Between the two fluid layers, diffusion and surface tension effects are ignored. The dimensional values are identified by the symbol $'$. The flow rate of saliva q'_1 is known and the flow rate of food bolus q'_2 is calculated. μ'_i refers to the viscosities (Pa.s) and σ'_2 to the surface tension of the food bolus with air (N/m).

$H'(x)$ refers to the half gap between the two cylinders, H'_0 its minimum, $h'_2(x)$ the location of the interface between the food bolus and the saliva, U' the cylinder velocity, L' the lift per unit of width, D' the drag per unit of width, $p'(x', y')$ the pressure field, R' the radius, $u'_1(x', z')$ the velocity field in the saliva, $u'_2(x', z')$ the velocity field in the food bolus and x'_m the split point abscise. The roll surface profiles are approximated by parabolas:

$$H'(x) = H'_0 + \frac{x'^2}{2R'} \tag{3}$$

The dimensionless values defined for imposed velocity and gap are given by:

$$x = \frac{x'}{\sqrt{2R'H'_0}}$$

$$z = \frac{z'}{H'_0}$$

$$u_i = \frac{u'_i}{U'}$$

$$q_i = \frac{q'_i}{U'H'_0}$$

$$p_i = \frac{p'_i H'_0}{\mu'_1 U'} \sqrt{\frac{H'_0}{2R'}}$$

$$L = \frac{L'H'_0}{\mu'_1 U' 2R}$$

$$D = \frac{D'H'_0}{\mu'_1 U' \sqrt{2R'H'_0}}$$

The dimensionless cylinder profile is given by:

$$H(x) = 1 + x^2 \tag{4}$$

The momentum conservation equations are solved in the lubrication approximation in their dimensionless form:

$$\frac{\partial p}{\partial x} = \frac{\partial^2 u_1}{\partial z^2} \tag{5}$$

$$\frac{\partial p}{\partial x} = \alpha \frac{\partial^2 u_2}{\partial z^2} \tag{6}$$

$$\frac{\partial p}{\partial z} = 0 \tag{7}$$

where α is the viscosity ratio:

$$\alpha = \frac{\mu'_2}{\mu'_1} \tag{8}$$

After changing the variables $\eta = z/H(x)$ and integration, we obtain:

$$u_1 = H^2(x)\frac{dp}{dx}\frac{\eta^2}{2} + A_1\eta + B_1 \tag{9}$$

$$u_2 = H^2(x)\frac{dp}{dx}\frac{\eta^2}{2} + A_2\eta + B_2 \tag{10}$$

where A_1, B_1, A_2, B_2 are integration constants. They are determined by considering no wall slip, continuity of velocity and shear stress at interface between the two fluids and symmetry. Defining $\beta = h_2(x)/H(x)$, the boundary conditions are:

$$u_1(\eta = 1) = 1 \tag{11}$$

$$u_1(\eta = \beta) = u_2(\eta = \beta) \tag{12}$$

$$\left.\frac{\partial u_1}{\partial \eta}\right|_{\eta=\beta} = \alpha \left.\frac{\partial u_2}{\partial \eta}\right|_{\eta=\beta} \tag{13}$$

$$\left.\frac{\partial u_2}{\partial \eta}\right|_{\eta=0} = 0 \tag{14}$$

We thus have:

$$u_1 = H^2(x)\frac{dp}{dx}\left(\eta^2 - 1\right) + 1 \tag{15}$$

$$u_2 = \frac{H^2(x)}{2}\frac{dp}{dx}\left[\frac{\eta^2}{\alpha} - 1 - \beta^2\left(\frac{1}{\alpha} - 1\right)\right] + 1 \tag{16}$$

After changing the variables $\theta = \arctan(x)$ and application of mass conservation, we have two equations on flow rates:

$$q_1 + q_2 - \frac{1}{\cos^2(\theta)} = \frac{1}{3\cos^4(\theta)}\frac{dp}{d\theta}\left[\beta^3\left(1 - \frac{1}{\alpha}\right) - 1\right] \tag{17}$$

$$q_2 - \frac{\beta}{\cos^2(\theta)} = \frac{1}{2\cos^4(\theta)}\frac{dp}{d\theta}\left[\beta^3\left(1 - \frac{2}{3\alpha}\right) - \beta\right] \tag{18}$$

Considering that upstream is fully submerged, we have:

$$p\left(\theta = -\frac{\pi}{2}\right) = 0 \tag{19}$$

We consider that the film splits at the first stagnation point, $\theta_m = \arctan(x_m)$ [38]:

$$p\left(\theta_m\right) = -\frac{1}{\alpha.Ca_m.r_m} \tag{20}$$

where r_m is the radius of curvature of the meniscus at the film-splitting point (Figure 4) and Ca_m is a modified capillary number:

$$Ca_m = \frac{\mu_2' U'}{\sigma_2'}\sqrt{\frac{2R'}{H_0'}} \tag{21}$$

If the meniscus is modelled as an arc of a circle between parallel plates of radius r_m, geometry and mass balance, geometry demands that [38]:

$$q_1 + q_2 + r_m = H\left(\theta_m\right) = 1 + \tan^2\left(\theta_m\right) \tag{22}$$

3.2. Resolution method

The problem was solved with Matlab7.0. For a set of parameters (q_1, α, Ca), we iterated on q_2 until the pressure output condition was verified (20). The ratio of (17) and (18) gives a polynomial equation of order 4 in β independent of the pressure:

$$\begin{aligned} 0 = & \frac{1 - 1/\alpha}{\cos^2(\theta)}\beta^4 \\ & + \left[\left(q_1 + q_2 - \frac{1}{\cos^2(\theta)}\right)\left(\frac{2}{3} - \frac{1}{\alpha}\right) - q_2\left(1 - \frac{1}{\alpha}\right)\right]\beta^3 \\ & + \left[-\frac{3}{2}\left(q_1 + q_2 - \frac{1}{\cos^2(\theta)}\right) - \frac{1}{\cos^2(\theta)}\right]\beta \\ & + q_2 \end{aligned} \tag{23}$$

The space was discretised into 4000 nodes. At each iteration and for each node, we determined the roots of (23) included between 0 and 1. The first stagnation point θ_m weas determined from equation (16) where $u_2 = 0$ for $\eta = 0$ and $\theta > 0$. So, we have to find the node satisfaying the following equation:

$$0 = \frac{1}{2cos(\theta_m)^2} \left.\frac{dp}{d\theta}\right|_{\theta=\theta_m} \left[-1 - \beta\left(\theta_m\right)^2 \left(\frac{1}{\alpha} - 1\right)\right] + 1 \tag{24}$$

(22) and (20) make it possible to calculate r_m and $p\left(\theta_m\right)$. Finally, we calculated the error ε on $p\left(\theta_m\right)$:

$$\varepsilon = \left\| \frac{p\left(\theta_m\right) - 1/Ca_m.r_m}{1/Ca_m.r_m} \right\| \tag{25}$$

We iterated on q_2 until $\varepsilon < 10^{-10}$. After resolution of this equation system, the resulting lift and the drag were calculated:

$$L = \int_{-\pi/2}^{\pi/2} \frac{p(\theta)}{\cos(\theta)^2}\,\mathrm{d}\theta \tag{26}$$

$$D = \int_{-\pi/2}^{\pi/2} \frac{1}{\cos(\theta)^2}\frac{dp}{d\theta}\,\mathrm{d}\theta \tag{27}$$

3.3. Gravity effects in experimental data

For the experimental data, gravity effects could not be avoided but could simply be included in the model. In the experiments, gravity acted from the negative x to the positive x. Considering that fluid densities are the same, the momentum conservation equations become:

$$\frac{\partial p_m}{\partial x} = \frac{\partial^2 u_1}{\partial z^2} \tag{28}$$

$$\frac{\partial p_m}{\partial x} = \alpha\frac{\partial^2 u_2}{\partial z^2} \tag{29}$$

where $p_m = p + St\left(x_0 - x\right)$ is the modified pressure. St is the Stokes number defined by:

$$St = H'^2_0 \rho.g/\mu_1 U' \tag{30}$$

where g is the acceleration due to gravity (10 m/s^2) and x_0 is the dimensionless free surface abscise from the minimum gap that can be calculated with the relationship $x_0 = x'_0/\sqrt{2.R.H'_0}$, where x'_0 is the dimension value (30 mm in the experiments). The solution method is the same as explained previously, but the pressure p is replaced by the modified pressure p_m.

4. Pharyngeal peristalsis simulator

In order to experimentally analyse the coating phenomena due to the pharyngeal peristalsis, an experimental set-up was developed. It is schematically depicted in Figure 5. It was composed of two rotating cylinders of 40 mm in radius. They are sufficiently wide to avoid side leakage (2x40 mm in width [28]). The radius value was estimated according to data on the evolution of the pharyngeal chamber geometry during swallowing given by Chang et al. [1]. A weak hydrophobic material for the cylinders was chosen in order to facilitate lubrication by saliva, Nylon6.6. A thin film of fluid simulating saliva was deposited on the cylinders by two slot coaters. The cylinder velocity was fixed at 0.2 m/s corresponding to physiological conditions (Table 1). The cylinders were equipped with scrapers and collectors and the gap was controlled with a transducer (0-250 µm). Scrappers were designed in order to carry out a total recovery of the coated bolus on the cylinders.

Newtonian glucose solutions and water were used as test fluids for the food bolus and the saliva respectively. In a first approach, since saliva viscosity is between 1 to 10 mPa.s [40], water was used to simulate it. To simulate the food bolus, glucose solutions were chosen for their Newtonian behaviour and their wide range of viscosity ($2.6\,10^{-2}$ and 0.4 Pa.s). The fluid temperature was controlled for each experiment. Viscosity was measured with a Physica MCR 301 (Anton Paar) at the experimental temperature (between 20-25°C).

Before a measurement was made, the deposited thickness of water was fixed and measured (40 µm). Velocity was imposed and water collected over a given time. The quantity of water allowed collected permited us to determine its flow rate and its thickness.

The glucose flow rate was determined with the measurement of the quantity of fluid passing through the contact during a known time (from 20 to 60 s).

Machining defects were measured (± 20 µm). For this, air was the test medium and the two cylinders were put in contact by application of a force (with a spring). The evolution of the distance seprating the axes of the cylinders was measured over several revolutions and provided machining defects. The experimental flow rate was obtained with the measurement of the quantity of glucose syrup passing through the contact m (in kg) during a known time t (in s). This flow rate was then adimensionalized by the velocity and the gap:

$$q = \frac{m}{2.\rho.t}\frac{1}{U'.H'_0} \tag{31}$$

where ρ is the density (kg/m^3). Considering that the uncertainties were principally due to the measurement of the gap and of the time, the uncertainty affecting the measurment of flow rate is:

$$\frac{\Delta q}{q} = \frac{\Delta H_0'}{H_0'} + \frac{\Delta t}{t} \tag{32}$$

where $\Delta H_0' = 20\,\mu m$ and $\Delta t = 1\,s$.

5. Results

5.1. Parametric study

Monolayer case

Numerical solutions were validated by comparing the results in the monolayer case with the analytical solution obtained by Coyle et al. [38]. Figure 6 shows that our numerical solutions correspond well to their analytical solutions. The dimensionless flow rate q_1 is independent of the modified capillary number when $Ca_m > 10$ and is equal to 1.3015. For low capillary numbers, Coyle et al. [38] showed that the flow rate is overestimated because the free-model surface is crude and there is recirculation occurs before the split region, which is not taken into account by the lubrication theory.

Food bolus flow rates

Figure 7-a shows that viscosity effects have a relatively low impact on food bolus flow rate q_2. There are two asymptotic cases: when α tends to zero or infinity, q_2 tends to two different constants depending on q_1. The variation is about 20%.

Figure 7-b represents the food bolus flow rate q_2 against the saliva flow rate q_1 for different values of viscosity ratios α. We observe two asymptotic cases. When there is no saliva at the interface ($q_1 = 0$), the bolus flow rate is constant regardless of the viscosity and q_2 is equal to 1.3015. When saliva fully floods the contact ($q_1 = 1.3015$), the bolus does not coat the mucosa ($q_2 = 0$). For $\alpha > 1$, we observe that q_2 reaches an maximum for the low values of q_1. After this maximum, q_2 decreases with q_1.

Pressure and surface profiles

This optimum is due to two antagonistic phenomena. The first is the fact that the contact obstruction by saliva is greater when q_1 increases and q_2 thus decreases. In fact, Figure 8-a shows the evolution of the interface location between the two fluids in the contact. When q_1 increases, the

obstruction by saliva is increasingly high. The second is due to the fact that the bolus shears the saliva thickness, especially since its viscosity is considerable, as shown in Figure 8-b, the velocity at the interface between the two fluids is faster and q_2 increases. Figure 8-c shows the characteristic pressure profile that is generated in the contact. The pressure steeply increases as the fluid is dragged into the narrowing channel, after which the channel widens and the pressure drops. Figure 8-c also reveals how it develops when the saliva flow rate falls.

Flow field distribution

Figure (9) presents flow field distributions and the location of the food bolus / saliva interface in the contact between the root of the tongue and the pharyngeal wall for different saliva flow rate at $\alpha = 100$ and $Ca_m = 10^3$. The velocity steeply increases as the fluid is dragged into the narrowing channel, after which the channel widens and the velocity decreases. The velocity is maximal at the axe of symmetry ($z = 0$) and minimal at the wall ($z = H(x)$). When the saliva flow rate q_1 increases, the food bolus velocity increases, but the obstruction of the contact by saliva increases too.

Generated forces

Lift and drag are represented in Figures 10-a and b compared to α for different values of q_1. In the case of a mono-layer of saliva ($q_2 = 0$ and $q_1 = 1.3015$), they are 0.32 and 0.9, respectively. These values correspond to those we can obtain from the analytical equations of Coyle et al. [38]. When there is no saliva at the interface ($q_1 = 0$), we have $L = 0.32\alpha$ and $D = 1.9\alpha$. When the contact is lubricated by saliva, the forces generated are included between these two asymptotic cases.

Finally, saliva reduces the influence of bolus viscosity on the generated forces and flow rates.

5.2. Experimental results

Experimental data are represented in Figure 11. Glucose syrup flow rate (bolus) is plotted against water flow rate (saliva) for two viscosity levels ($2.6\,10^{-2}$ Pa.s and 0.4 Pa.s).

The uncertainties are greater when q_1 increases, because these data are obtained for small gaps and the machning defects are considerable compared to the gap (cf. §4). We observe that the non-lubricated points for glucose syrups and water are close to the theoretical value of 1.3. Non-lubricated points for water have been established with a small gap in order to avoid effects of gravity, explaining the high level of uncertainties. Gravity effects cannot be avoided for lubricated data but

can simply be included in the model (cf. §3.3). Each data set was modelled and the comparison with experimental data and numerical results are given in Figure 11. The maximal value of the Stokes number St representing gravity effects on viscous effects is 0.58. This observation confirms that gravity could not be ignored in the experiments and that the flow was not dominated by gravity. Figure 11 show that experimental results are in agreement with model predictions. For high viscosity and high levels of lubrication, the measured flow rates are greater than those predicted. For this data, we observed that a large quantity of water came back up and dissolved the glucose syrups during measurement. In the case of a large gap, the mixing of glucose syrups by water was very low. We can hypothesize that when lubrication is considerable, the flow becomes unstable and recirculations are generated as observed.

Numerical results are therefore in agreement with experimental data when saliva flow rates and viscosity ratios are relatively low. The lubrication theory is thus an effective tool for modeling these phenomena. When they were high, model predictions were underestimated compared to experimental results. We can assume that in these cases instabilities and recirculation could occur because the saliva film is very confined and sheared. Saliva thickness has a strong influence on the results and its relative importance could change the nature of the flow.

In conclusion, the experimental results validate the bilayer lubrication model developed in this study.

6. Application to flavour release and discussion

6.1. Qualitative applications to swallowing

We now qualitatively analyse the influence of saliva and food bolus viscosity on aroma release. In the first section of this article, we concluded that the hypothesis of constrictor muscles working at imposed load and drag is - although speculative - reasonable. The previously results obtained can be easily rearranged in order to consider that a given force is applied to the cylinders. Calculation details are given in the appendix. Figure 12 represents dimensionless residual food bolus thickness t_2 compared to dimensionless initial saliva thickness t_1 for different viscosity ratios α at imposed load and drag. When there is no saliva at the interface, bolus thickness is constant regardless of the viscosity ($t_2 = 0.036$) and when saliva thickness fully floods the contact ($t_1 = 0.036$) , the bolus does not coat the mucosa. Between these extremes, when saliva thickness and viscosity increase, bolus thickness decreases.

6.2. Application to flavour release

As mentionned in the introduction, the role of viscosity on flavour release has to be clarified. To be perceived, aroma compounds must be released from the food bolus to reach the olfactory receptors. Many authors agree that short term aroma persistence (<1 min) is due to food coating on the pharyngeal mucosa [9, 41, 42]. The goal of this section is to analyse the influence of viscosity on aroma release from a rheological point of view, independently of other mechanisms, via the product layer thickness.

Considering that the contact is fully flooded by saliva and the food bolus, the area of the deposited film is constant regardless of the viscosity, and only the film thickness can vary. The main transport phenomenon of aroma compounds in the thin film is diffusion. In the air, the molecules are stripped by breathing. Based on a dimensional analysis as proposed by Weel at al. [15], the characteristic time τ (s) of aroma compound depletion in the coating film is in first approximation given by $\tau \sim t'^2_2/D_a$, with t'_2 the residual food bolus thickness (in m) and D_a the aroma diffusion coefficient in the fluid (typically 10^{-9} m^2/s for aroma compounds in water). Hence, a variation of the product thickness induces a variation of the characteristic time of the depletion that we refer to as the "persistence." Figure 13 illustrates the influence of the thickness on the dynamic profile of aroma release. These data are the predictions of a mechanistic model based on the one developed by Trelea et al. [9] (Doyennette et al., in preparation).

In terms of aroma release, if the contact is not fully flooded by saliva, the decrease of the food bolus thickness with an increase of viscosity (Figure 12) induces a decrease of aroma persistence when viscosity increases independently of physicochemical properties, i.e. D_a is constant. For example, the characteristic time of the "persistence" is divided by 4 between viscosity ratios of 1 and 3 and for a saliva thickness of 0.02. If saliva fully floods the contact ($t_1 > 0.036$), the coating can be due to interdiffusion, mixing or instabilities. Finally two sets of conditions can be distinguished depending on the value of t_1. The first is characterised by a relatively thin layer of saliva; food bolus viscosity has a strong influence on mucosa coating and, therefore, on flavour release. The second is obtained when the layer of saliva is relatively thick; the mucosa coating must be due to a hydrodynamic mixing with saliva, diffusion or instabilities.

6.3. Quantitative application

In this section, the results are quantitatively applied. In the first part of this article, we gave the order of magnitude of the lift applied by the constrictors and the peristaltic wave velocity, but

we have no data on the applied drag (Table 1). Knowing the applied load and the wave velocity, we can estimate the thickness of saliva necessary to fully flood the contact (corresponding to the monolayer case). From the dimensionless expressions of the lift L' and the thickness t', we can deduce the following relationship: $t' = t.\mu_1.U'.2.R.L/L'$ where U' is the wave velocity (= 0.2 m/s), R the radius (= 40mm, estimated from [1]), μ_1 the saliva viscosity (= 5mPa.s) and L' the applied load (= 10N/m). The values of t and L are those obtained when the contact is fully flooded by food bolus (1.3 and 0.32 respectively). We observe that the initial thickness of saliva should be lower than 3.3 µm for the bolus to coat the mucosa. This value seems quite small, but no value of saliva thickness coating mucosa is given in the literature to our knowledge. It should be emphasized that the calculations were performed with rigid cylinders that migth result in the underestimation of this thickness. To improve model predictions, it would be interesting to take mucosa deformability into account.

Finally, this type of biomechanical model, combined with a mechanistic model for in vivo aroma release, could be a relevant tool to help formulate food in order to obtain specific dynamic profiles of aroma release or products adapted to people who suffer from swallowing disorders.

Acknowledgements

The authors gratefully acknowledge the French National Research Agency (ANR) project « SensIn-Mouth » for its financial support.

Appendix

For a given lift L' and drag D',the dimensionless variables are:

$$z = \frac{z'}{(D'/L')^2 .2R}$$

$$x = \frac{x'}{2R'.D'/L'}$$

$$u = \frac{u'}{D'^2/\mu_1' L'}$$

$$p = \frac{p'}{L'^2/2R'.D'}$$

$$q = \frac{q'}{2R'.D'^4/\mu'_1 L'^3}$$

We have two conditions for the dimensionless lift and the drag: $L = 1$ and $D = 1$. The values at given gap and velocity and the variables at a given lift and drag are identified by "a" and "b" respectively. The dimension flow rate can be expressed in two ways:

$$q'_i = U'.H'_0.q^a_i \tag{33}$$

$$q'_i = \frac{2R'D'^4}{\mu'_1 L'^3} q_i^2 \tag{34}$$

By equalising the two relationships and replacing L' and D' with $L^a = \frac{L'H'_0}{\mu'_1 U' 2R'}$ and $D^a = \frac{D'H'_0}{\mu'_1 U' \sqrt{2R'H'_0}}$, we have:

$$q^b_i = q^a_i.L^{a\,3}/D^{a\,4} \tag{35}$$

In the same way, we determine the cylinder velocity:

$$U^b = U^a.L^a/D^{a\,2} \tag{36}$$

where $U^a = 1$. The deposited layer t_i is given by the flow rate divided by the cylinder velocity:

$$t^b_i = q^a_i \left(\frac{L^a}{D^a}\right)^2 \tag{37}$$

On the basis of this relationship, we can easily plot the dimensionless deposited thickness of the food bolus t_2 against the initial thickness of saliva t_1 for different viscosity ratios α. However, it should be observed that the modified capillary number is not constant. In fact, the boundary pressure condition at the contact output becomes:

$$p^b(\theta_m) = -\frac{1}{\alpha.Ca^b_m.r_m}$$

with $Ca^b_m = D'/\sigma_2$.

Hence, we obtain a relationship between the modified capillary number at a given velocity and gap an therefore, a given lift and drag : $Ca^b_m = D^a.Ca^a_m$.

Since Ca^a has a low impact on the results (cf. 5.1), the fact that C_m^b is not constant has a little influence on the results. These manipulations make it possible to supplementary numerical resolution.

References

[1] M. Chang, B. Rosendall, B. Finlayson, Mathematical modeling of normal pharyngeal bolus transport: A preliminary study, Journal of Rehabilitation Research and Development 35 (3) (1998) 327–334.

[2] Y. Meng, M. Rao, A. Datta, Computer simulation of the pharyngeal bolus transport of Newtonian and non-Newtonian fluids, Food and Bioproducts Processing 83 (C4) (2005) 297–305.

[3] H. Mizunuma, M. Sonomura, S. K., H. Ogoshi, S. Nakamura, N. Tayama, Numerical modeling and simulation on the swallowing of jelly, Journal of Texture Studies 40-4 (2009) 406–426.

[4] M. Nicosia, J. Robbins, The fluid mechanics of bolus ejection from the oral cavity, Journal of Biomechanics 34 (12) (2001) 1537–1544.

[5] R. de Wijk, J. Prinz, A. Janssen, Explaining perceived oral texture of starch-based custard desserts from standard and novel instrumental tests, Food Hydrocolloids 20 (1) (2006) 24–34.

[6] K. Mathmann, W. Kowalczyk, H. Petermeier, A. Baars, M. Eberhard, A. Delgado, A numerical approach revealing the impact of rheological properties on mouthfeel caused by food, International Journal of Food Science and Technology 42 (6) (2007) 739–745.

[7] J. Strassburg, A. Burbidge, A. Delgado, C. Hartmann, Geometrical resolution limits and detection mechanisms in the oral cavity, Journal of Biomechanics 40 (16) (2007) 3533 – 3540.

[8] M. A. Nicosia, A planar finite element model of bolus containment in the oral cavity, Computers in Biology and Medicine 37 (10) (2007) 1472–1478.

[9] I. C. Trelea, S. Atlan, I. Deleris, A. Saint-Eve, M. Marin, I. Souchon, Mechanistic mathematical model for in vivo aroma release during eating of semiliquid foods, Chemical Senses 33 (2) (2008) 181–192.

[10] K. Mathmann, W. Kowalczyk, A. Delgado, Development of a hybrid model predicting the mouthfeel of yogurt, Journal of Texture Studies 40 (1) (2009) 16–35.

[11] M. Levine, Radiology of the esophagus, WB Saunders, Philadelphia, 1989.

[12] A. Buettner, A. Beer, C. Hannig, M. Settles, Observation of the swallowing process by application of videofluoroscopy and real-time magnetic resonance imaging-consequences for retronasal aroma stimulation, Chemical Senses 26 (9) (2001) 1211–1219.

[13] T. Hollowood, R. Linforth, A. Taylor, The effect of viscosity on the perception of flavour, Chemical Senses 27 (7) (2002) 583–591.

[14] D. Cook, T. Hollowood, R. Linforth, A. Taylor, Oral shear stress predicts flavour perception in viscous solutions, Chemical Senses 28 (2003) 11–23.

[15] K. Weel, A. Boelrijk, J. Burger, V. M., H. Gruppen, A. Voragen, G. Smit, New device to simulate swallowing and in vivo aroma release in the throat from liquid and semiliquid food systems, Journal of Agricultural and Food Chemistry 52 (21) (2004) 6564–6571.

[16] A. Saint-Eve, N. Martin, H. Guillemin, E. Semon, E. Guichard, I. Souchon, Flavored yogurt complex viscosity influences real-time aroma release in the mouth and sensory properties, Journal of Agricultural and Food Chemistry 54 (20) (2006) 7794–7803.

[17] D. Cook, R. Linforth, A. Taylor, Effects of hydrocolloid thickeners on the perception of savory flavors, Journal of Agricultural and Food Chemistry 51 (10) (2003) 3067–3072.

[18] S. Hamlet, J. Choi, M. Zormeier, F. Shamsa, R. Stachler, J. Muz, L. Jones, Normal adult swallowing of liquid and viscous material: Scintigraphic data on bolus transit and oropharyngeal residues, Dysphagia 11 (1) (1996) 41–47.

[19] H. C. A. Bogaardt, J. J. Burger, W. J. Fokkens, R. J. Bennink, Viscosity is not a parameter of postdeglutitive pharyngeal residue: Quantification and analysis with scintigraphy, Dysphagia 22 (2) (2007) 145–149.

[20] A. M. Kelly, K. Macfarlane, K. Ghufoor, M. J. Drinnan, S. Lew-Gor, Pharyngeal residue across the lifespan: a first look at what's normal, clinical Otolaryngology 33 (4) (2008) 348–351.

[21] U. Pivk, N. P. Ulrih, M.-A. Juillerat, P. Raspor, Assessing lipid coating of the human oral cavity after ingestion of fatty foods, Journal of Agricultural and Food Chemistry 56 (2) (2008) 507–511.

[22] M. Donner, J. Bosma, D. Robertson, Anatomy and physiology of the pharynx, Gastrointestinal Radiology 10 (3) (1985) 196–212.

[23] B. Jones, Radiographic evaluation of motility of mouth and pharynx, GI Motility Online

[24] R. Goyal, H. Mashimo, Physiology of oral, pharyngeal, and esophageal motility, GI Motility Online

[25] R. Dantas, M. Kern, B. Massey, W. Dodds, P. Kahrilas, J. Brasseur, I. Cook, I. Lang, Effect of swallowed bolus variables on oral and pharyngeal phases of swallowing, American Journal of Physiology 258 (5, Part 1) (1990) G675–G681.

[26] A. Pal, R. Williams, I. Cook, J. Brasseur, Intrabolus pressure gradient identifies pathological constriction in the upper esophageal sphincter during flow, American Journal of Physiology-Gastrointestinal and Liver Physiology 285 (5) (2003) G1037–G1048.

[27] H. Gregersen, Biomechanics of the gastrointestinal tract, Springer, 2003.

[28] B. Hamrock, S. Schmid, B. Jacobson, Fundamentals of fluid film lubrication, Secon edition, McGraw-Hill Companies, 2004.

[29] R. Williams, A. Pal, J. Brasseur, I. Cook, Space-time pressure structure of pharyngo-esophageal segment during swallowing, American Journal of Physiology-Gastrointestinal and Liver Physiology 281 (5) (2001) G1290–G1300.

[30] M. Nicosia, J. Brasseur, A mathematical model for estimating muscle tension in vivo during esophageal bolus transport, Journal of Theoretical Biology 219 (2) (2002) 235–255.

[31] P. Pouderoux, P. Kahrilas, Deglutitive tongue force modulation by volition, volume, and viscosity in humans, Gastroenterology 108 (5) (1995) 1418–1426.

[32] G. Ali, T. Laundl, K. Wallace, D. Shaw, D. deCarle, I. Cook, Influence of mucosal receptors on deglutitive regulation of pharyngeal and upper esophageal sphincter function, American Journal of Physiology 267 (1994) 644–649.

[33] R. Dantas, B. Massey, M. Kern, I. Cook, W. Dodds, Effect of bolus volume and viscosity on the pharyngeal phase of swallowing, Gastroenterology 95 (3) (1988) 861.

[34] V. Raut, G. McKee, B. Johnston, Effect of bolus consistency on swallowing - does altering consistency help?, European Archives of Oto-Rhino-Laryngology 258 (1) (2001) 49–53, 71st Annual Meeting of the German-Society-for-Oto-Rhino-Laryngology-Head-and-Neck-Surgery/4th European Congress of Oto-Rhino-Laryngology-Head-and-Neck-Surgery (EUFOS), Berlin, Germany, May 13-18, 2000.

[35] S. Takeuchi, H. Tohara, H. Kudo, K. Otsuka, H. Saito, H. Uematsu, K. Mitsubayashi, An optic pharyngeal manometric sensor for deglutition analysis, Biomedical Microdevices 9 (6) (2007) 893–899.

[36] H. Taniguchi, T. Tsukada, S. Ootaki, Y. Yamada, M. Inoue, Correspondence between food consistency and suprahyoid muscle activity, tongue pressure, and bolus transit times during the oropharyngeal phase of swallowing, Journal of Applied Physiology 105 (3) (2008) 791–799.

[37] T. Tsukada, H. Taniguchi, S. Ootaki, Y. Yamada, M. Inoue, Effects of food texture and head posture on oropharyngeal swallowing, Journal of Applied Physiology 106 (6) (2009) 1848–1857.

[38] D. Coyle, C. Macosko, L. Scriven, Film-splitting flows in forward roll coating, Journal of Fluid Mechanics 171 (1986) 183–207.

[39] A. Hannachi, E. Mitsoulis, Numerical analysis of multilayer forward roll coating, Journal of Plastic Film and Sheeting 6(3) (1990) 170–190.

[40] R. G. Schipper, E. Silletti, M. H. Vinyerhoeds, Saliva as research material: Biochemical, physicochemlical and practical aspects, Archives of Oral Biology 52 (12) (2007) 1114–1135.

[41] K. Wright, B. Hills, T. Hollowood, R. Linforth, A. Taylor, Persistence effects in flavour release from liquids in the mouth, International Journal of Food Science and Technology 38 (3) (2003) 343–350.

[42] V. Normand, S. Avison, A. Parker, Modeling the kinetics of flavour release during drinking, Chemical Senses 29 (3) (2004) 235–245.

[43] R. German, J. Palmer, Anatomy and development of oral cavity and pharynx, GI Motility Online.

List of Tables

1 Physiological variables and approximate corresponding value. 26

List of Figures

1 Anatomy of the oral cavity and the pharynx (adapted from [43]) 27

2 Swallowing sequences. Phase 1: Initiation of swallowing. Phase 2: Pharyngeal peristalsis (adapted from [26]) 28

3 Scheme of the peristaltic wave and associated study system. Near the most occluded point, the pharyngeal walls are in rotation one compared to the other. In black, $\left(\overrightarrow{x'}, \overrightarrow{z'}\right)$ represents the laboratory frame, whereas, in grey, $\left(\overrightarrow{X'}, \overrightarrow{Z'}\right)$ represents the wave frame. 29

4 Schematic diagram of definitions and notations. 30

5 Pharyngeal peristalsis simulator: (1) saliva feed, (2) slot coater, (3) food bolus, (4) scraper, (5) collector. 31

6 Dimensionless flow rate as a function of modified capillary number in the monolayer case. Comparison with the analytical results of Coyle et al. [38]. 32

7 Dimensionless food bolus flow rate as a function of the viscosity ratio α for different saliva flow rates q_1 (a) and as a function of the saliva flow rate q_1 for different viscosity ratios α (b) at imposed gap and velocity ($Ca_m = 1000$). 33

8 Location of the interface between the food bolus and saliva h_2 (a), velocity at the interface between the food bolus and saliva (b), and pressure profile p (c), for different dimensionless saliva flow rates q_1 and for a viscosity ratio α of 100 ($Ca_m = 1000$). . 34

9 Example of flow field distribution (isovalues of velocity) in the contact and saliva / food bolus interface (withe line) for $q_1 = 0$ and $q_2 = 1.30$ (a), $q_1 = 0.1$ and $q_2 = 1.41$ (b) ,$q_1 = 0.3$ and $q_2 = 1.20$ (c), ($\alpha = 100$ and $Ca_m = 1000$). 35

10 Dimensionless lift L (a) and drag D (b) as a function of the viscosity ratio α for different saliva flow rates q_1 at imposed gap and velocity ($Ca_m = 1000$). 36

11 Glucose flow rate as a function of water flow rate for two viscosity levels (solid symbols) at imposed gap and velocity. Each piece of data has been modelled by taking gravity effects into account (hollow symbols). 37

12 Dimensionless food bolus thickness t_2 as a function of saliva thickness t_1 for different viscosity ratio a at a given force (lift and drag). 38

13 Evolution f the concentration in aroma compound C_N in the nasal cavity for different residual thicknesses of product t_2': a decrease of the thickness induces a decrease of the "persistence" (from Doyennette et al., in preparation). 39

Table 1: Physiological variables and approximate corresponding value.

Description	Symbol	Typical value	References
Saliva thickness	t_1'	no data	
Wave velocity	U'	0.1-0.5 m/s	[1, 2, 25]
Radius	R	40 mm	estimated from [1]
Load	L'	10-60 N/m	estimated from [29]
Drag	D'	no data	
Saliva viscosity	μ_1'	1-10 mPa.s	[40]
Bolus viscosity	μ_2'	>1 mPa.s	

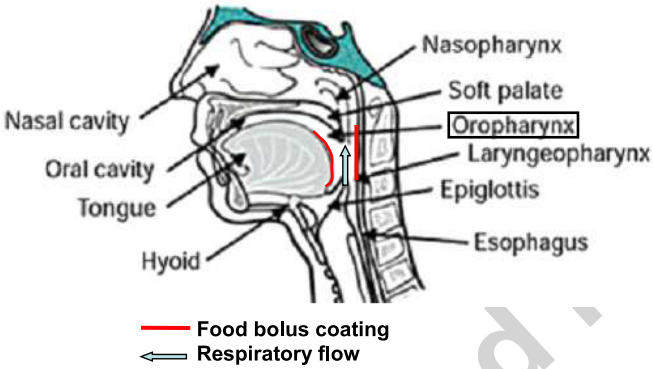

Figure 1: Anatomy of the oral cavity and the pharynx (adapted from [43])

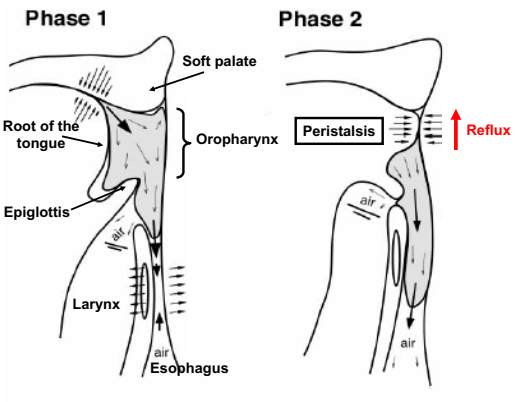

Figure 2: Swallowing sequences. Phase 1: Initiation of swallowing. Phase 2: Pharyngeal peristalsis (adapted from [26])

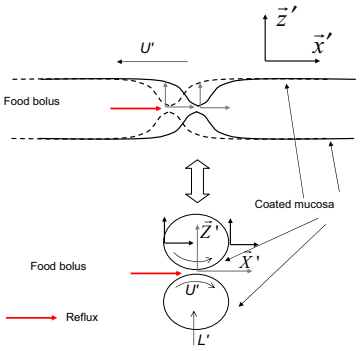

Figure 3: Scheme of the peristaltic wave and associated study system. Near the most occluded point, the pharyngeal walls are in rotation one compared to the other. In black, $\left(\overrightarrow{x'}, \overrightarrow{z'}\right)$ represents the laboratory frame, whereas, in grey, $\left(\overrightarrow{X'}, \overrightarrow{Z'}\right)$ represents the wave frame.

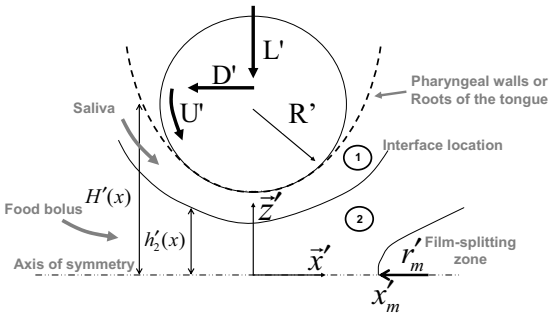

Figure 4: Schematic diagram of definitions and notations.

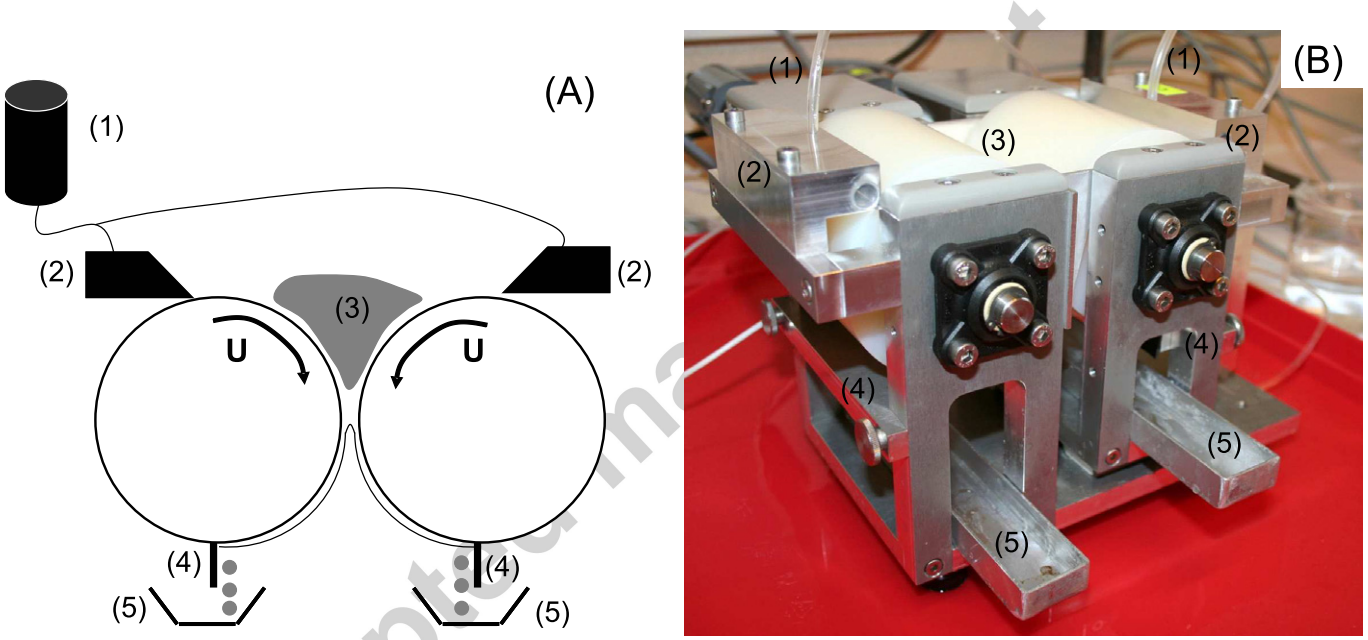

Figure 5: Pharyngeal peristalsis simulator: (1) saliva feed, (2) slot coater, (3) food bolus, (4) scraper, (5) collector.

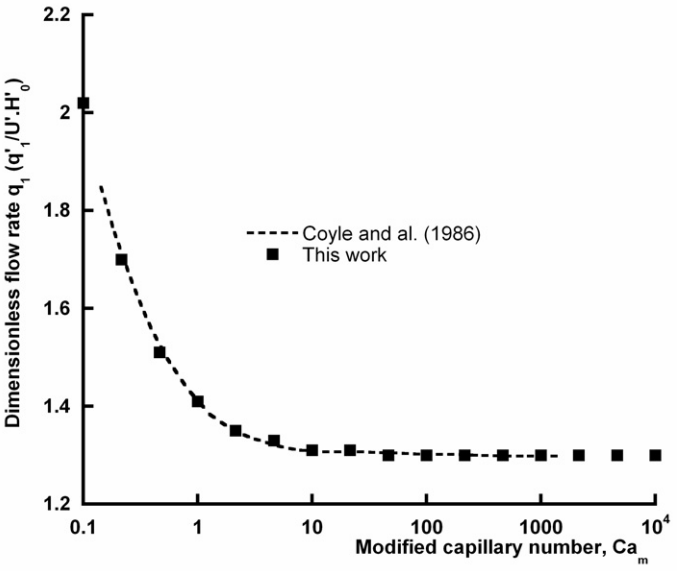

Figure 6: Dimensionless flow rate as a function of modified capillary number in the monolayer case. Comparison with the analytical results of Coyle et al. [38].

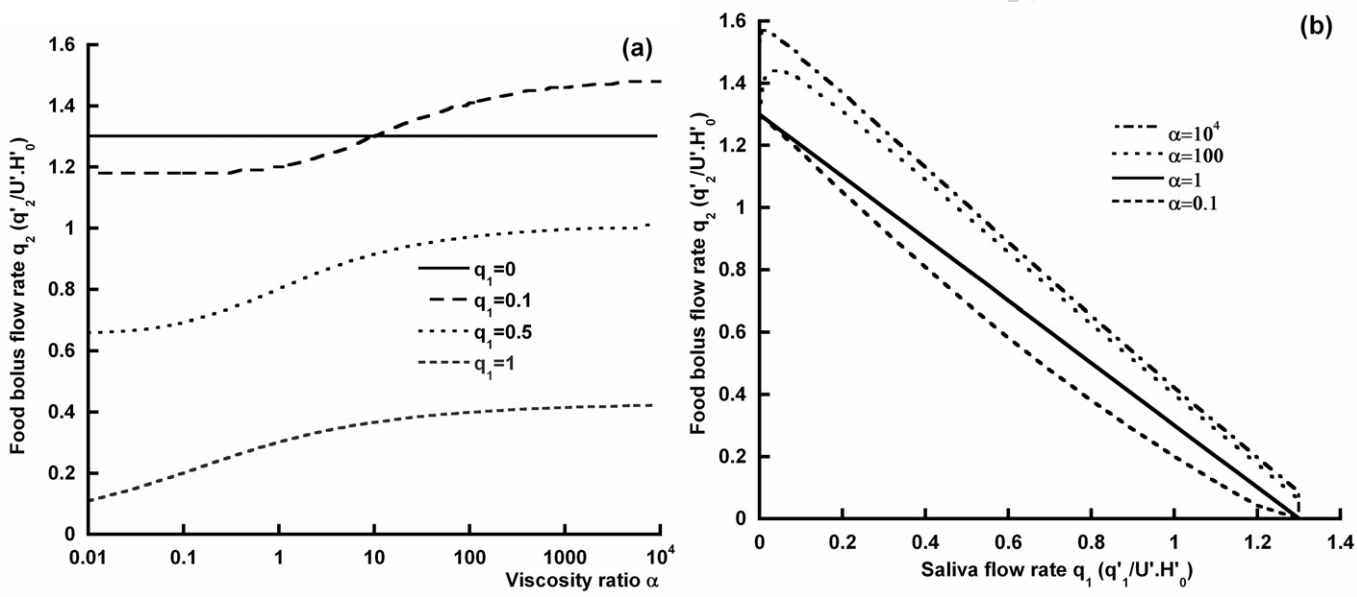

Figure 7: Dimensionless food bolus flow rate as a function of the viscosity ratioα for different saliva flow rates q_1 (a) and as a function of the saliva flow rate q_1 for different viscosity ratios α (b) at imposed gap and velocity ($Ca_m = 1000$).

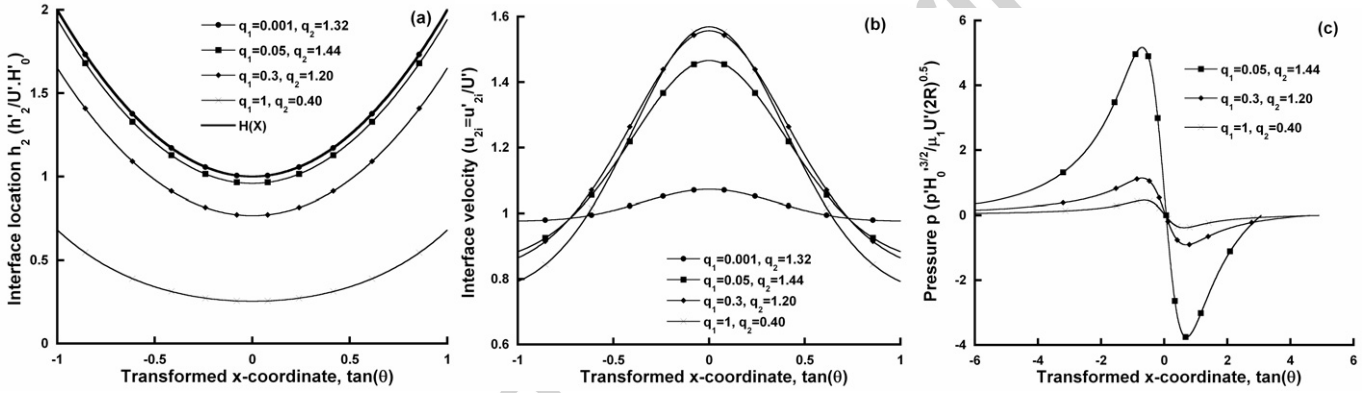

Figure 8: Location of the interface between the food bolus and saliva h_2 (a), velocity at the interface between the food bolus and saliva (b), and pressure profile p (c), for different dimensionless saliva flow rates q_1 and for a viscosity ratio α of 100 ($Ca_m = 1000$).

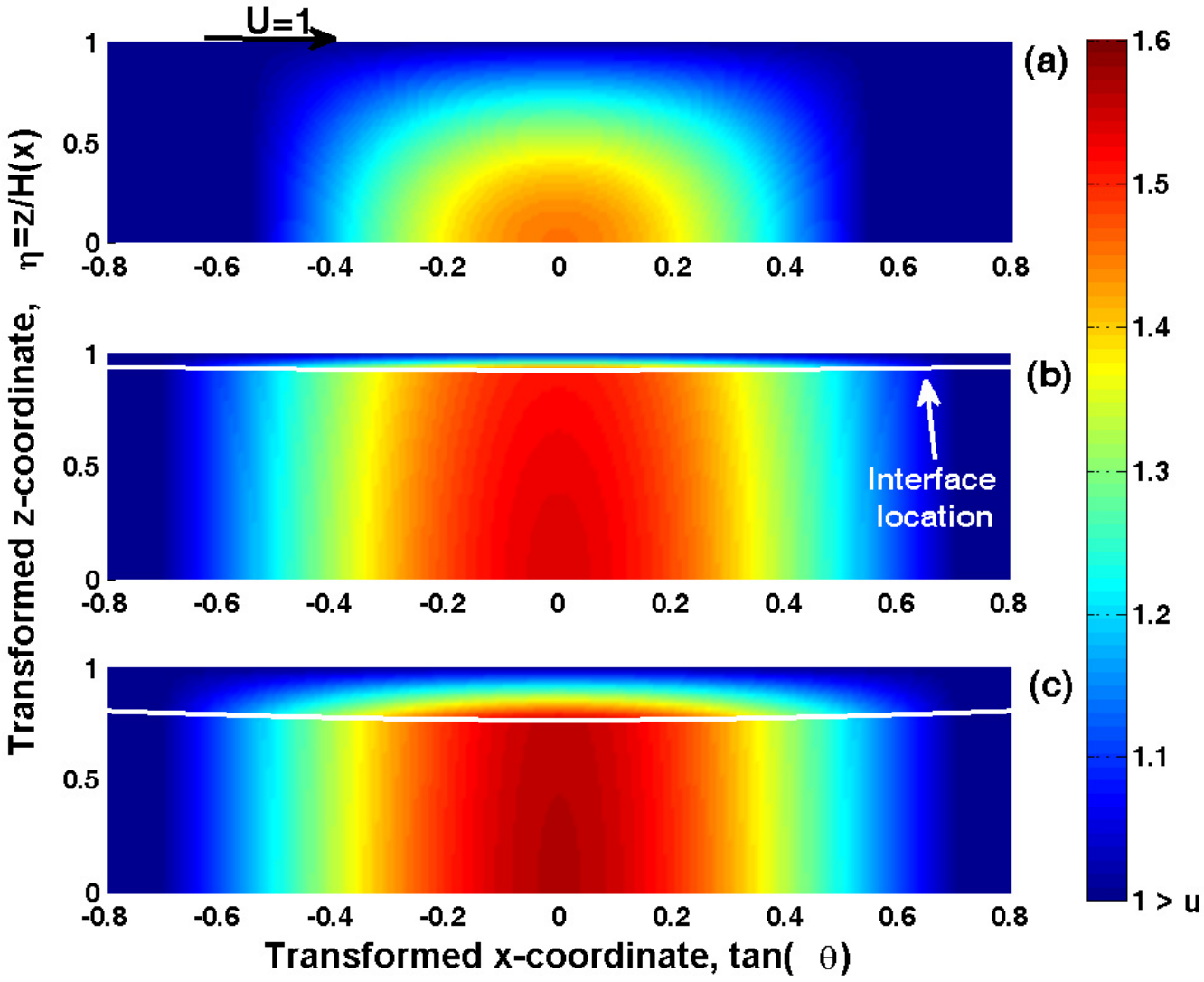

Figure 9: Example of flow field distribution (isovalues of velocity) in the contact and saliva / food bolus interface (withe line) for $q_1 = 0$ and $q_2 = 1.30$ (a), $q_1 = 0.1$ and $q_2 = 1.41$ (b) ,$q_1 = 0.3$ and $q_2 = 1.20$ (c), ($\alpha = 100$ and $Ca_m = 1000$).

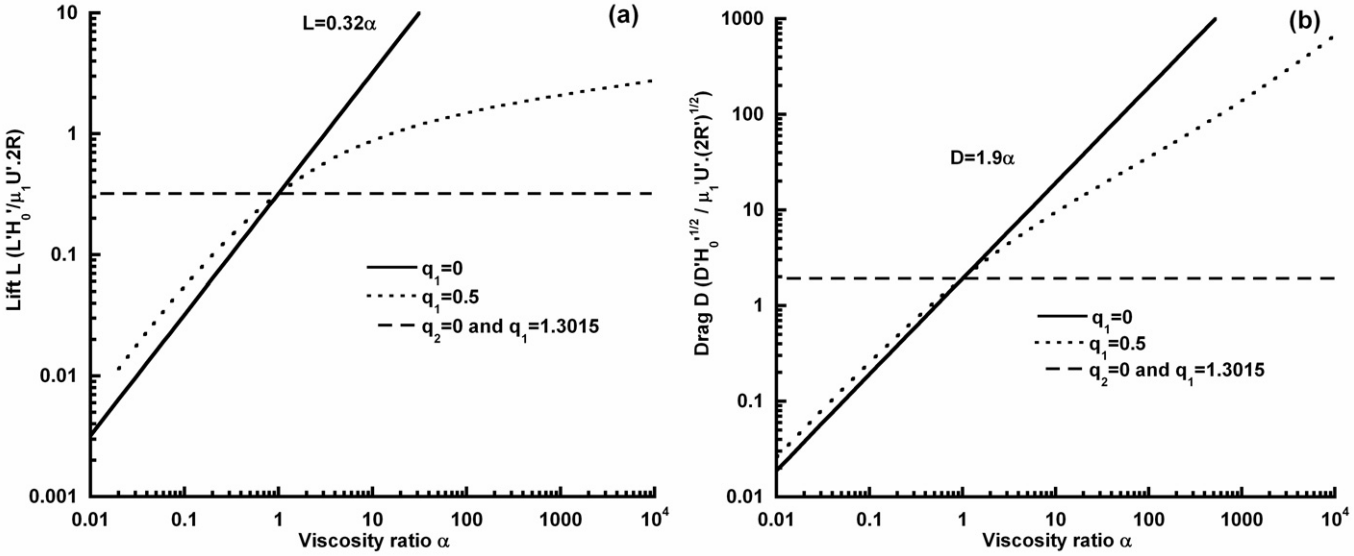

Figure 10: Dimensionless lift L (a) and drag D (b) as a function of the viscosity ratio α for different saliva flow rates q_1 at imposed gap and velocity ($Ca_m = 1000$).

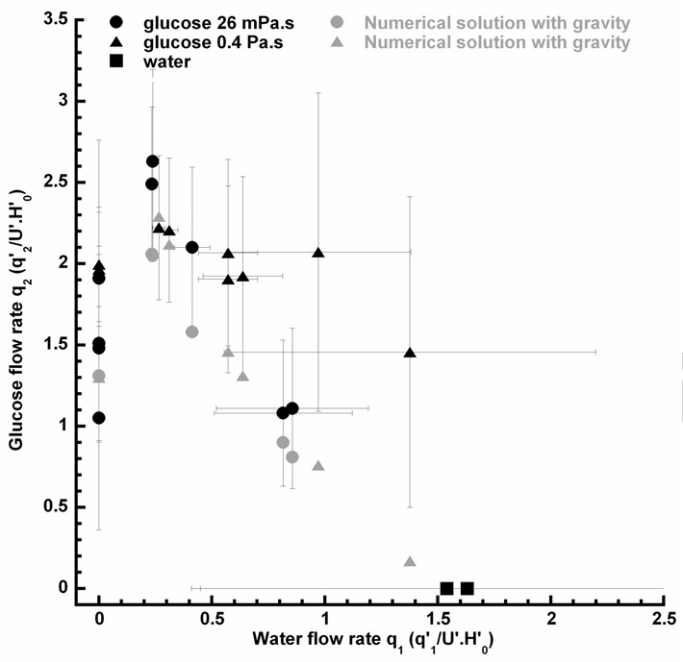

Figure 11: Glucose flow rate as a function of water flow rate for two viscosity levels (solid symbols) at imposed gap and velocity. Each piece of data has been modelled by taking gravity effects into account (hollow symbols).

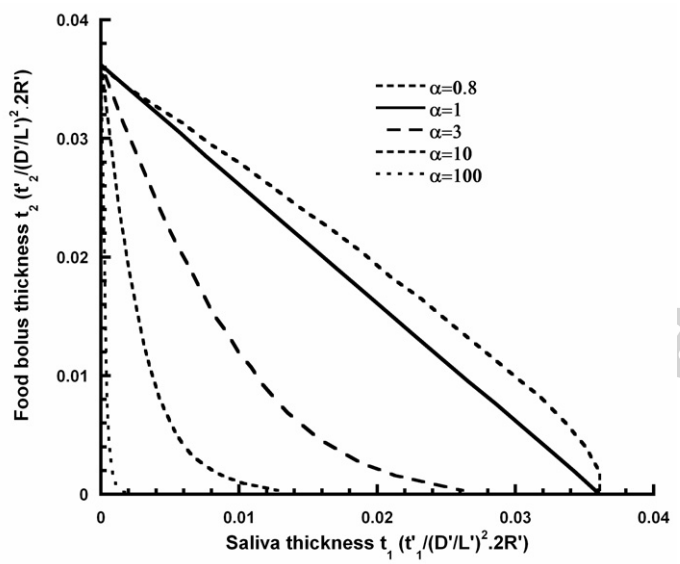

Figure 12: Dimensionless food bolus thickness t_2 as a function of saliva thickness t_1 for different viscosity ratio α at a given force (lift and drag).

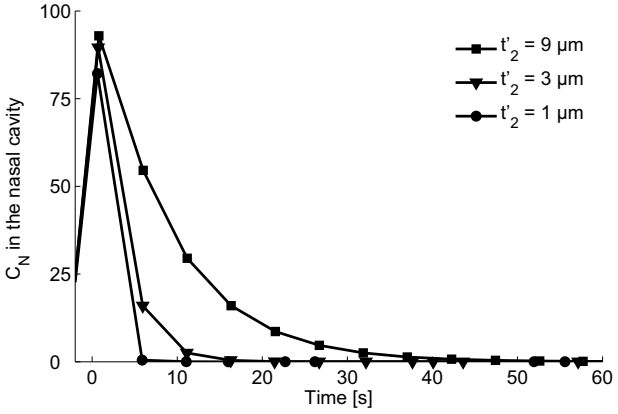

Figure 13: Evolution f the concentration in aroma compound C_N in the nasal cavity for different residual thicknesses of product t'_2: a decrease of the thickness induces a decrease of the "persistence" (from Doyennette et al., in preparation).